Thermal stress-induced charge and structure heterogeneity in emerging cathode materials

Judith Alvarado,[1‡] Chenxi Wei,[2,3‡] Dennis Nordlund,[3] Thomas Kroll,[3] Dimosthenis Sokaras,[3] Yangchao Tian[2], Yijin Liu,[3*] Marca M. Doeff[1*]

1. Energy Storage & Distributed Resources Division, Lawrence Berkeley National Laboratory, Berkeley, California 94720, USA

2. National Synchrotron Radiation Laboratory, University of Science and Technology of China, Hefei, Anhui 230027, China

3. Stanford Synchrotron Radiation Lightsource, SLAC National Accelerator Laboratory, Menlo Park, California 94025, USA

* email: liuyijin@slac.stanford.edu, mmdoeff@lbl.gov

‡ These authors contributed equally to the paper

Abstract

Nickel-rich layered oxide cathode materials are attractive near-term candidates for boosting the energy density of next generation lithium-ion batteries. The practical implementation of these materials is, however, hindered by unsatisfactory capacity retention, poor thermal stability, and oxygen release as a consequence of structural decomposition, which may have serious safety consequences. The undesired side reactions are often exothermic, causing complicated electro-chemo-mechanical interplay at elevated temperatures. In this work, we explore the effects of thermal exposure on chemically delithiated $LiNi_{0.8}Mn_{0.1}Co_{0.1}O_2$ (NMC-811) at a practical state-of-charge (50% of Li content) and an over-charged state (25% lithium content). A systematic study using a suite of advanced synchrotron radiation characterization tools reveals the dynamics thermal behavior of the charged NMC-811, which involves sophisticated structural and chemical evolution; e.g. lattice phase transformation, transition metal (TM) cation migration and valence change, and lithium redistribution. These intertwined processes exhibit a complex 3D spatial heterogeneity and, collectively, form a valence state gradient throughout the particles. Our study sheds light on the response of NMC-811 to elevated temperature and highlights the importance of the cathode's thermal robustness for battery performance and safety.

Keywords: lithium-ion battery; cathode; Ni-rich NMC; thermal stability

1.1 Introduction

The potentially enormous electric vehicle market has bolstered the need for lithium-ion battery (LiB) systems with improved performance. In particular, there are stringent requirements for developing next generation battery materials that meet the specifications for commercial applications; e.g. high specific energy, high energy density, stable cycle life, low cost, and improved safety. Of the next generation battery cathode materials, nickel (Ni)-rich NMC ($LiNi_xMn_yCo_zO_2$; $x+y+z\approx1$, $x\geq y+z$) layered oxide cathodes are regarded as the best near-term candidates because of their high practical energy densities. Depending on their Ni content and the voltage limits used, the practical capacity can reach beyond 200 mAh/g.[1,2] Another benefit is that the higher Ni content reduces the amount of cobalt used in the cathode. This is important both for reasons of cost and because of the dubious ethics of cobalt mining.[3] Although these are considerable incentives to use Ni-rich NMCs, these materials suffer from unsatisfactory capacity retention upon cycling and poorer structural stability than the widely studied $LiNi_{1/3}Mn_{1/3}Co_{1/3}O_2$ (NMC-333).[4,5] Upon charging, the extraction of lithium (Li) causes significant phase transformations that diminish performance, especially at high states-of-charge (SOC).[6] Moreover, the poor thermal stability of the partially or fully delithiated Ni-rich NMCs is another concern.

While increasing the Ni content results in higher practical energy densities, it also critically influences the thermal stability and safety. [7,8] In a LiB, there are several possible exothermic reactions that can occur. Examples include: 1) chemical reduction/oxidation of the electrolyte by the anode and cathode, 2) thermal decomposition of the solid electrolyte interphase, 3) thermal decomposition of the anode, and 4) thermal decomposition of the cathode. [9–11] Understanding the effects of Ni content on cathodic thermal stability is of the utmost importance, because of the potential for thermal runaway, particular at high SOC. Charging to high potentials may increase practical energy density but the cathode material becomes more reactive when deeply delithiated. To overcome this in commercial battery modules, a battery management system is used to prevent overcharging. For example, in commercial $LiCoO_2$ (LCO) batteries, an upper cutoff voltage of 4.2V is often used in order to maintain at least 50% of Li in the structure for the sake of the LiB's longevity. Overcharging LCO to higher potentials can result in LCO lattice collapse and release of gaseous oxygen.[11,12] With this in mind, researchers have focused on studying the effects of thermal exposure on overcharged (>0.5 Li content) cathode materials such as $LiNi_{0.8}Co_{0.15}Al_{0.05}O_2$ (NCA), various NMC compositions, and lithium nickel oxide. [13]

To this end, combining synchrotron x-ray diffraction (XRD) with transmission electron microscopy (TEM) to correlate structure evolution upon thermal

exposure, Wu *et al.* determined that when the lithium content of NCA was below 0.3, the particle contained three main phases (rhombohedral core, a spinel shell, and a rock-salt structure) when heated from room temperature to 450°C, whereas NMC-333 with 0.3 Li content primarily contained M_3O_4 spinel type phase when heated to 533°C.[8] This series of materials was further investigated under harsher conditions (601°C) by Nam *et al.* using several synchrotron characterization techniques.[14] In both sets of materials, the Ni and Co change valence state as a consequence of thermal treatment while the Mn is largely not affected. [14] In NMCs, as the Ni content increases the probability of rocksalt formation increases, causing significant oxygen to be released.[15,16] The above-mentioned studies used electrochemical cycling to remove lithium from the host structure and the electrodes were all charged to the same potential regardless of the nominal cathode composition. Because these materials exhibit different voltage profiles, their SOC differed as a result. Furthermore, the results were complicated by the presence of carbon and binder in the electrodes, which may participate in the reactions. Grent et al. demonstrated that electrochemical delithiation can cause non uniformity in Ni oxidation states due to secondary particle size morphology, electrode fabrication, and battery cycling conditions.[17] Here, we aimed to extend and complement these previous studies, using model systems that eliminated the complications from other electrode components to investigate the behavioral changes as a function of depth by leveraging both hard and soft X-ray techniques.

While efforts have been devoted to understand the effects of thermal exposure on an over charged Ni-rich NMC cathode, little is known about the thermal stability of NMCs that contain 50% lithium in the structure, close to the composition reached at the end of charge under normal cycling conditions. Because of the relevance to both normal cell operation and overcharge, the thermal stabilities of both $Li_xNi_{0.8}Mn_{0.1}Co_{0.1}O_2$ at x=0.5 and 0.25 were investigated as a function of Li content herein.

1.2 Materials and Methods

1.2.1. Materials Synthesis and Chemical Delithiation

Synthesis of $LiNi_{0.8}Mn_{0.1}Co_{0.1}O_2$ (abbreviated hereafter as NMC-811) was conducted using a coprecipitation method. First, stoichiometric amounts of Ni $(NO_3)_2 \cdot 6H_2O$ (Sigma Aldrich), Co $(NO_3)_2 \cdot 6H_2O$ (Sigma Aldrich) and Mn $(NO_3)_2 \cdot 4H_2O$ (Sigma Aldrich) were added to deionized water to make a 0.4M transition metal salt solution. A 0.2M ammonium hydroxide solution was prepared and used to maintain optimal pH during titration. Both the ammonium hydroxide solution and transition metal solution were titrated to a 0.8M lithium hydroxide solution (at constant stirring) using a Thermal Scientific cartridge pump at a speed of 1 mL/minute. The transition metal hydroxide precipitate was collected, washed with deionized water, filtered by

centrifuge, and dried under vacuum at 100°C for 12 hours. The dried transition metal hydroxide powder was milled with SPEX sample prep mixer/ mill 8000M for 30 minutes with a 10% excess of lithium hydroxide monohydrate (Sigma Aldrich). This mixture was calcined in an oxygen environment at 500ºC for 5 h using a ramp rate of 5 ºC min^{-1} then at 850ºC for 10 h (5 ºC min^{-1}).

To prepare the chemically delithiated samples, the pristine powders were mixed with 0.05M NO_2BF_4 in acetonitrile media using stoichiometric ratios, while constantly stirring for 24 hours, in an argon filled glovebox. The delithiated powders were then washed with acetonitrile four times between each centrifugation to remove any unreacted residue of NO_2BF_4. The powder was directly transferred to a vacuum oven attached to the glovebox to dry at room temperature for 12 hours, thus avoiding any air exposure.

1.2.2. Characterization

The pristine and chemically delithiated powders were dissolved in concentrated nitric acid and analyzed by inductively coupled plasma optical emission spectrometer (ICP-OES, Varian ICP-OES 720 Series) to determine the chemical composition. Scanning electron microscopy (SEM) was performed on a JEOL JSM-7000F with a Thermo Scientific energy dispersive X-ray spectroscopy (EDS) detector. Thermogravimetric analysis (TGA) was performed with a Perkin-Elmer Pyris 1 TGA instrument under nitrogen using a heating rate of 5 °C/minute.

Temperature-controlled XRD analysis was performed using a Panalytical X'Pert Pro diffractometer with monochromatized Cu Kα radiation equipped with an Anton Parr HTK 1200 hot stage. Scans were collected between 15 and 75° (2θ) at a rate of 0.0001°/s and a step size of 0.022°. The chemically delithiated NMC-811 powders were heated in a purged argon environment at a ramp rate of 5 °C/minute and the temperature was held for one hour before acquiring XRD patterns.

Samples for the ex-situ thermal studies using hard x-ray absorption spectroscopy (XAS or XANES) were prepared using the Anton Parr HTK 1200 hot stage. After heating, they were sealed with kapton tape in an argon filled glovebox and placed in aluminum pouches for transfer. All measurements were carried out in both transmission and fluorescence modes at beamline 2-2 at Stanford Synchrotron Radiation Lightsource (SSRL). Calibration was applied to all spectra using the first inflection point of the corresponding Ni, Mn or Co metal foil. XANES data were analyzed with Athena software.

In-situ X-ray Raman spectroscopy (XRS) experiments were conducted at beamline 6-2b at SSRL. First, 250 mg of each sample were pressed into pellets and loaded into the sample chamber. The Ni L-edge and O K-edge were measured after samples were heated to 120°C and 300°C (temperature held for 1 hour) by using the 40-crystal x-ray Raman spectrometer (with an

energy resolution of ~0.45eV using the Si(660) mode) and an incident X-ray beam of ~150x400 μm^2 monochromatized with a Si(311) monochromator. [33]

Samples for the ex-situ soft XAS thermal studies were prepared similarly to those for the hard XAS experiments. The previously heated samples were mounted onto aluminum sample holders with double-sided carbon tape in an argon-filled glove box, placed into a sealed jar contained within another jar and transferred to a glove bag purged with argon connected to the XAS load-lock chamber. Measurements were conducted on the beamline 10-1 at SSRL, using a 31-pole wiggler and a spherical grating monochromator with 20 mm entrance and exit slits, a 0.2 eV energy resolution and a 1 mm^2 beam spot. Data were collected at room temperature under ultrahigh vacuum (10^{-9} Torr) using the total electron yield (TEY) and fluorescence yield (FY) mode detectors.

The full field transmission X-ray microscopy (FF-TXM) two- and three-dimensional XANES experiments were conducted at beamline 6-2c of SSRL. Pristine and chemically delithiated powders were loaded into quartz capillary tubes with diameters of 100 μm and wall thicknesses of 10 μm. A stack of transmission images, with nominal spatial resolution of ~30 nm, were recorded as the energy of the incoming X-rays was scanned across the Ni K-edge and Co K-edge. In the near edge region, the energy step was set to be 1 eV for sufficient energy resolution. Over the pre-edge and post edge regions, we scanned the energy at a larger step size of 10 eV in order to cover a wide energy window for normalization of the x-ray absorption spectra. After initial data reduction using an in-house developed software package (TXM-Wizard), we effectively recovered over 20 million XANES spectra with each one of them associated with a unique pixel in the image. The shape of the spectra represents the local chemical fingerprints and can be used to quantify the Ni and Co oxidation state over the corresponding pixels.

1.3 Results and discussion

1.3.1. Material properties and chemical delithiation

The NMC-811 powders shown in Figure S1 were synthesized by coprecipitation. The secondary particles are comprised of agglomerated large primary particles ranging in size from 1 to 2 μm. Inductively coupled plasma optical emission spectrometry (ICP-OES) validated the materials composition, indicating that the transition metal ratios were consistent with the targeted values. The pristine NMC-811 is phase pure and the reflections of the XRD pattern confirms its layered structure; all reflections could be indexed to the $R\bar{3}m$ space group (Figure S2). The (003)/(104) intensity ratio of 1.40 suggests that the structure is well ordered with minimal ion-mixing. The resulting materials were subject to chemical delithiation as described in

the methods section. The lithium (Li) contents were close to the targeted values based on the molar concentrations of the oxidant.

Figure S2 shows the XRD pattern of the 50% delithiated NMC-811. The (003) reflection shifted to a lower angle and developed a slight shoulder, as did the (104) reflection. These changes are indicative of a conversion from the H1 phase to a phase mixture of H2 and H3. This is similar behavior to what is seen for the $LiNiO_2$ system[13], where the H2 phase appears at approximately 50% electrochemical delithiation.[18,19] For the 75% delithiated sample, reflections due to the H3 phase are more pronounced, as demonstrated by the increased intensity of the (003) shoulder peak located at higher angles. The doubling of the (101), (104), and (110) reflections are due to the presence of two phases and is consistent with literature findings for Ni-rich cathode materials at this particular Li content.[20,21] In spite of the biphasic nature of the delithiated materials, the layered structure is maintained with minimal cationic mixing, as demonstrated by the (003)/(104) peak intensity ratios, as well as the clear resolution of the doublet peaks at 64.5°.

1.3.2. Temperature-controlled XRD

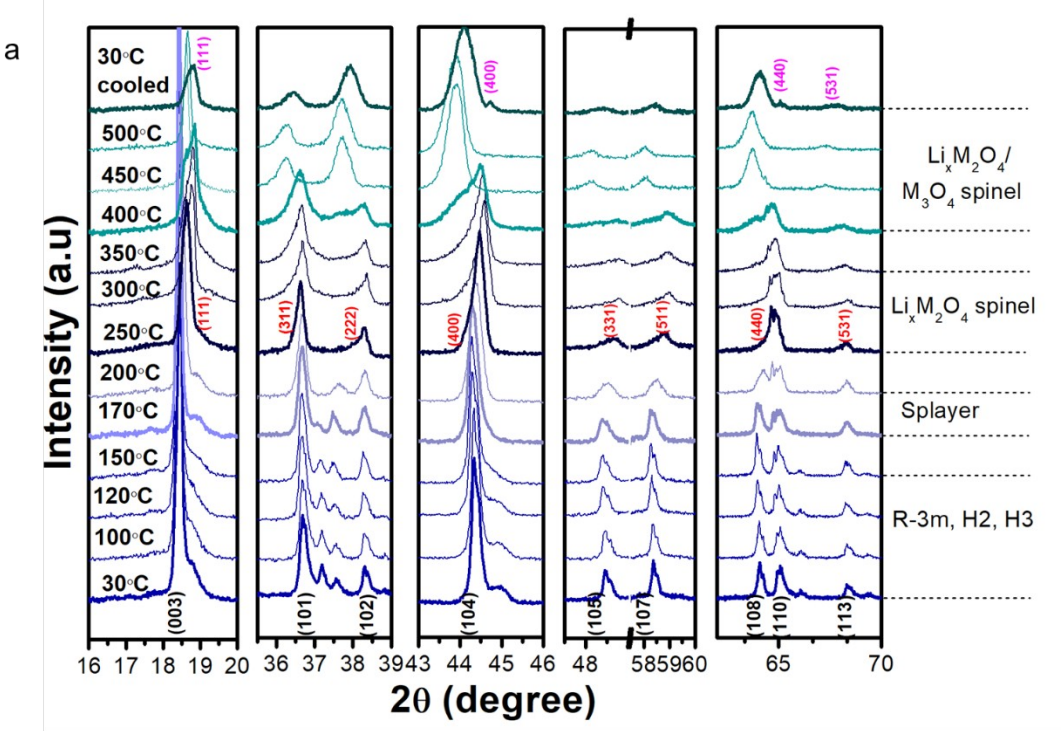

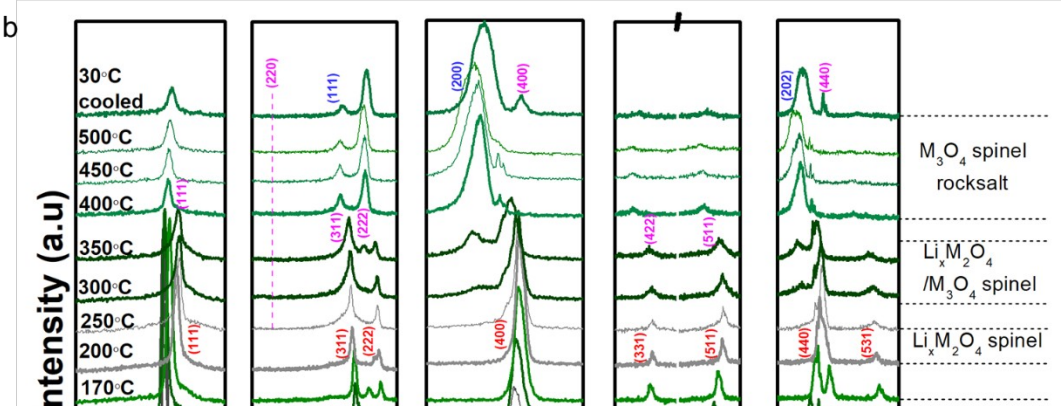

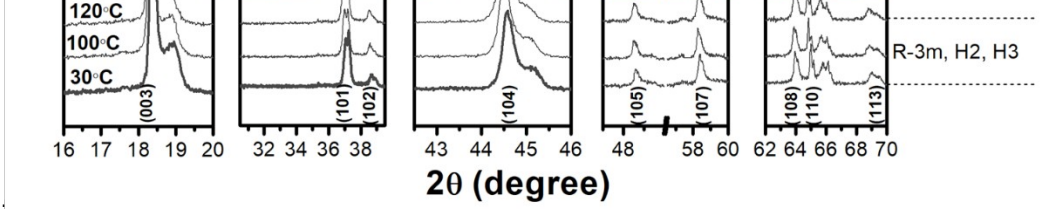

Figure 1. In-situ x-ray diffraction patterns of (a) 50% chemically delithiated NMC-811 (b) 75% delithiated NMC-811 heated to 500°C. Phase changes are indicated to the right of each set of patterns. Reflections diagnostic of $Li_xM_2O_4$ (s1) are shown in red, M_3O_4 (s2) in pink, and rock salt (r) in blue.

The thermally-driven structural evolution of the delithiated NMC powders was examined using in-situ temperature-controlled XRD (Figure 1). For the 50% delithiated sample, there were negligible changes between 30°C and 150°C and a mixture of layered and $Li_xM_2O_4$ spinel phase formed between 170°C and 200°C, identified as "splayered". At 250°C, the splayered structure converted to disordered $Li_xM_2O_4$ spinel (s1, $Fd\bar{3}m$), with this phase transition reaching completion at 450°C, as evidenced by the merging of the (108) and (110) peaks to form the (440_{s1}) peak. In addition, the (003) reflection shifted and broadened to form the (111_{s1}) peak. After the sample was cooled to 30°C, (400_{s2}) and (440_{s2}) reflections diagnostic of an M_3O_4 spinel phase (s2) emerged, and the intensity of the (111_{s2}) peak decreased. The final product after cooling is a mixture of a minority M_3O_4 phase and a $Li_xM_2O_4$-type spinel majority phase, with considerable structural disorder for the latter, as evidenced by the peak broadening. For this sample, there was no evidence of rocksalt formation in the temperature range that was studied. Conversely, the 75% delithiated sample underwent a splayered transition between 150°C to 170°C, as evidenced by the significant reduction in intensity of the H3 peaks and (104) peak broadening as it converted to the $Li_xM_2O_4$ (400_{s1}) peak. At 200°C, the H3 phase began the transition to the $Li_xM_2O_4$ spinel phase and formation of the M_3O_4 spinel phase was nearly complete at 350°C. Figure S3 shows the evolution of the (220_{s2}) peak, starting at 250°C. The transition at 350°C was complicated by concomitant formation of rocksalt (MO) as evidenced by the (111_r) reflection appearing as a broad shoulder on the ($311_{s1/s2}$) reflection. The formation of rock salt was complete by 400°C, and at 500°C the 75% delithiated sample is primarily composed of M_3O_4 spinel phase as well as rocksalt and $Li_xM_2O_4$ spinel phases. After the material is cooled to room temperature, there are no additional phase transitions, indicating irreversibility. Both the formation of M_3O_4 spinel phase and rock salt involve oxygen release, with the amount dependent on the exact stoichiometries of these compounds (e.g., rock salt phases may contain lithium). Thermogravimetric analysis (TGA) was used to quantify the amount of oxygen loss during heating to 600°C (Figure S4). The TGA is broadly consistent with the structural information in the XRD temperature-controlled experiments, showing losses beginning near 250°C. For the 50% delithiated sample, little M_3O_4 spinel phase is formed and there is only an 8.5% weight loss overall. However, the 75% delithiated sample lost 13% percent of its original weight, consistent with the observation of significant M_3O_4 spinel and rocksalt phase conversion. It is worth noting that once the materials are chemically delithiated, any lithium carbonate present in the samples is completely removed (see supporting information).[22] Furthermore, the materials were carefully dried and stored under inert atmosphere, so that

this weight loss is not attributable to water [14], and must be due solely to oxygen loss.

1.3.2 Transition metal K-edge observations

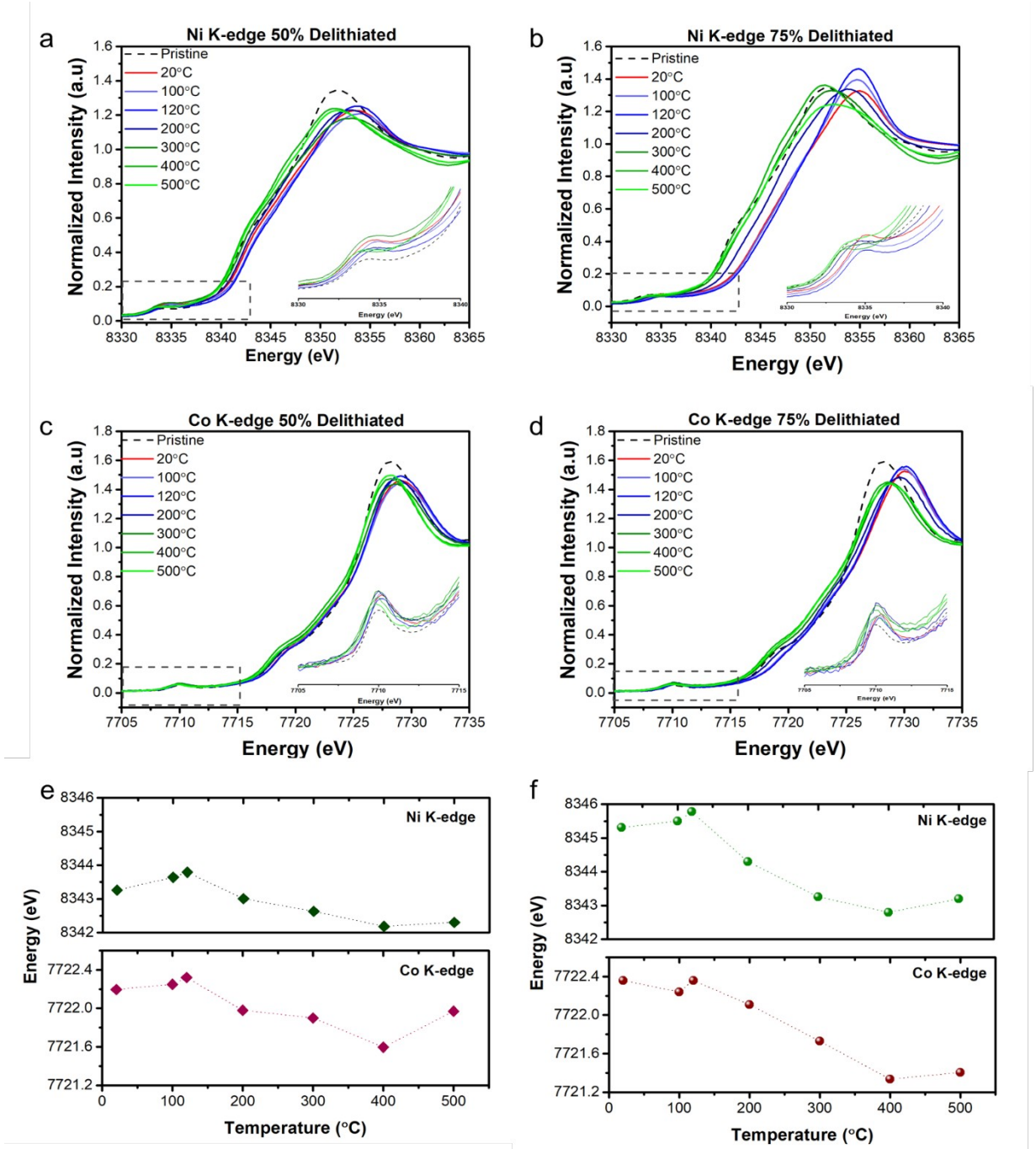

Figure 2. Post heating x-ray absorption spectroscopy XANES measurements at the Ni K-edge and Co K-edge of the (a, c) 50 % delithiated (b, d) 75% delithiated samples, respectively, after heating to the indicated temperatures. Edge shift of each element as a function of temperature is given for (e) 50% delithiated and (f) 75% delithiated samples.

The bulk structural transformations to progressively less oxygen-rich phases upon heating should result in a lowering of the average transition metal (TM) valence state, but the in-situ XRD experiments do not offer information about which metals undergo reduction. X-ray absorption near edge spectroscopy (XANES) provides insights into the electronic structure changes and TM metal local environments in the bulk materials. At higher valence states, the core electrons have a stronger bond to the nucleus requiring higher photon energies for photoionization to occur. Conversely, a shift to lower energy is correlated with lower oxidation states of the TM. Figure 2 a and b show the changes of Ni XANES energies as function of temperature for the two different delithiated samples, using edge positions at 50% intensity values. Both samples behave similarly; there is actually a slight apparent increase in oxidation state as the temperature is raised to 120˚C Above this temperature, the Ni is progressively reduced as the temperature is increased to 500°C, as also seen with NCA materials. [51] Somewhat similar behavior is seen for Co as a function of temperature in both samples. Figures 2 e and f plot relative edge positions (measured at half the normalized intensity) for both Co and Ni for the two samples, where the trends of increased oxidation state, followed by progressive reduction can be readily observed. The apparent paradox of metal oxidation seen at temperatures below the point where any phase conversion was detected is difficult to explain, particularly because air was rigorously excluded for all of these experiments, so that there was no source of oxidant. This more likely reflects changes in the covalencies or bond lengths of the TM-O bonds rather than true oxidation. [23,24]

The pre-edge peaks also contain information about metal coordination. The increase in intensity of the pre-edge peak near 7710 eV in the Co XANES as the temperature is raised indicates a suppression of centrosymmetry.[14] This suggests a change from octahedral (centrosymmetric) to tetrahedral (non-centrosymmetric) coordination as conversion to M_3O_4 spinel occurs, indicating that Co migrates to the tetrahedral sites. This is particularly apparent for the 75% delithiated sample, where there is more conversion to M_3O_4 spinel than in the 50% delithiated sample. In contrast to Ni and Co, the Mn K-edge XANES experiment (Figure S5), shows little change, indicating that Mn remains in the tetravalent state as the samples are heated.

1.3.3. Transition metal L-edge and oxygen K-edge observations

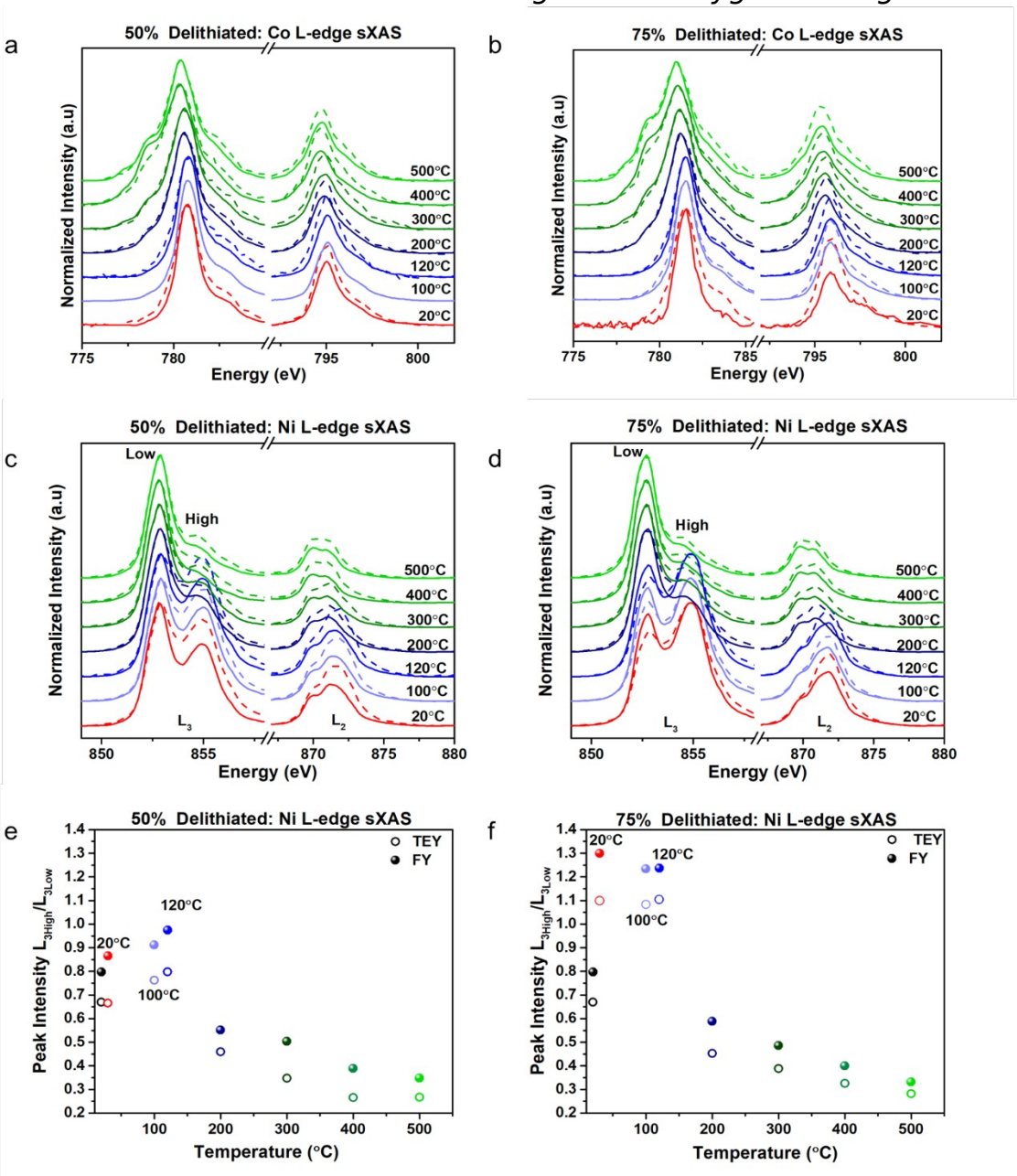

Figure 3. Post heating soft x-ray absorption spectroscopy measurements of the Co and Ni L-edges of the (a, c) 50 % delithiated and (b, d) 75% delithiated samples. TEY mode data is shown as solid lines and FY mode data as dashed lines. The relative intensity ratio L_{3high}/L_{3low} as a function of temperature in both TEY mode (open circles) and FY mode (solid circles) are shown in (e) for 50% and (f) for 75% delithiated samples.

In contrast to transition metal K-edge XAS, which probes the bulk, soft XAS probes surface and sub-surface regions of the samples, depending on

detection mode. In the experiments described here, fluorescence yield (FY) mode penetrates approximately 100 nm into the sample, and total electron yield (TEY) mode about 5-10 nm in. Soft XAS is commonly used to investigate the dipole allowed electron excitations stemming from 2p to 3d states known as the L-edge; this includes the $2p_{3/2}$ (L_3) and $2p_{1/2}$ (L_2) spin orbit states. [25,26] These specific excitations can be used as fingerprints for valence state, spin state, and chemical bonding states.

Figure S6 shows the Ni, Co, and Mn L-edge data for the pristine and two chemically delithiated samples prior to heating, in both TEY and FY modes. As previously described, the primary particles of the pristine NMC-811 are 1-2 µm, larger than the penetration depth of FY mode (Figure S1). In the case of Ni, the increase in the relative L_{3high}/L_{3low} intensity ratios for the delithiated materials is evidence of oxidation. For Co, slight shifting of peaks to higher energies indicates that Co was also oxidized. A comparison of the FY and TEY data for the pristine NMC-811 indicates that Ni and Co are more reduced at the surface than deeper into the samples. This is due to surface reconstruction to rocksalt, resulting in a TM oxidation state gradient from the surface into the bulk.[21,27,28] This discrepancy is less pronounced for the chemically delithiated samples, although there is still some evidence of surface reconstruction.[22] Consistent with the hard XAS measurements, little change was observed for Mn. In this regard, NMC-811 behaves much like NMC-111, which has a higher Mn content and less Ni. [8,14] Mn was not further examined in this study, as it appears to undergo little change under the conditions studied here.

Ex situ soft XAS Ni and Co L-edge results on the heated delithiated samples as a function of temperature are presented in Figure 3. Figures 3 a and d show evidence of reduction of Co after heating, as seen by the appearance of large shoulders at lower energies on the main Co L_3 edge features. This appears at about 300°C for the 50% delithiated sample, coinciding with the formation of the $Li_xM_2O_4$ spinel phase shown in the temperature controlled XRD (Figure 1a) and consistent with the Co XAS K-edge spectra (Figure 2b. While no oxygen loss is required to form $Li_{0.5}M_2O_4$ in principle, off-stoichiometric compositions (e.g., those that are oxygen-deficient) appear to form under these conditions (also see TGA results in Figure S4 showing onset of oxygen loss near 300˚C for this sample). The shoulder increases for both samples above 400°C and there is a slight overall shift of the L_3 peak to lower energy. At these higher temperatures, there is evidence for M_3O_4 spinel phase formation in the bulk and significant oxygen loss, which requires reduction of TM. A comparison between Figure 3 a and b suggests that reduction of Co is more pronounced in the 75% delithiated sample compared to the 50% delithiated sample, evident by the higher intensity of the L_3 shoulder and the data in the temperature-controlled XRD.

Figures 3c and d shows the Ni L-edge spectra for the 50 % delithiated and 75% delithiated samples as a function of temperature, respectively.

Consistent with the pristine sample, the Ni ions present on surfaces of the NMC delithiated particles are more reduced than in the bulk, regardless of Li content and thermal exposure, although the discrepancies diminish somewhat for samples treated at higher temperatures. Based on the L_{3high}/ L_{3low} intensity ratios (Figures 3e and f), both the samples show a slight apparent increase in the Ni oxidation state from 20 °C to 120°C at both the surface and sub-surface regions. While covalency effects and bond length changes may partially explain these results, as with the hard XAS, the observed differences between surface and sub-surface regions also suggest that increased Li mobility at elevated temperatures resulted in local compositional and redox state heterogeneities. Above 200°C, the Ni is progressively reduced, with the surface Ni at lower oxidation states than at the sub-surface at every temperature.

Oxygen K-edge XAS spectra contain two regions: (1) the local intensity maxima (between 528-535ev) related to the O 1s transition to TM3d-O2p hybridized states and (2) the high energy region above 535eV corresponding to the O 1s transitions to hybridized TM 4sp-O2p states. Given that the first region primarily pertains to the effect of oxygen on the TM 3d band, we focused our analysis on this region. See Figure S7 for spectra in both FY and TEY modes on pristine and delithiated samples prior to heating.[21,29,30] Note that a strong peak near 534 eV in the TEY spectrum of the pristine (as-

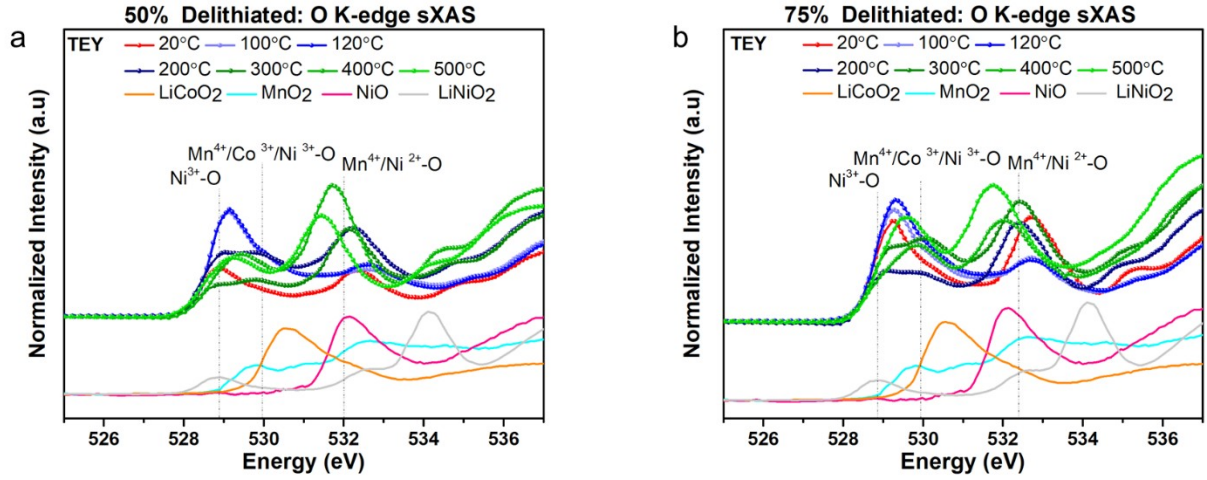

Figure 4. Post heating soft x-ray absorption spectroscopy O K-edge spectra in the TM 3d-O2p region in TEY mode for the (a) 50 % delithiated and (b) 75% delithiated samples. The spectra of several standard materials are also presented.

made) NMC is absent from the FY spectrum (i.e., the sub-surface region) and also from the delithiated samples. Although a peak for Ni^{3+}-O coincides with this, as observed in the reference spectrum of $LiNiO_2$, it is more likely to belong to a carbonate species, given the observed behavior. It is common for a thin layer of Li_2CO_3 to be present on Ni-rich cathodes,[13] thin enough to

be detectable in TEY mode, but not in FY mode. The chemical delithiation process removes this layer.

Figure 4 presents the TEY data for the delithiated NMCs heated to different

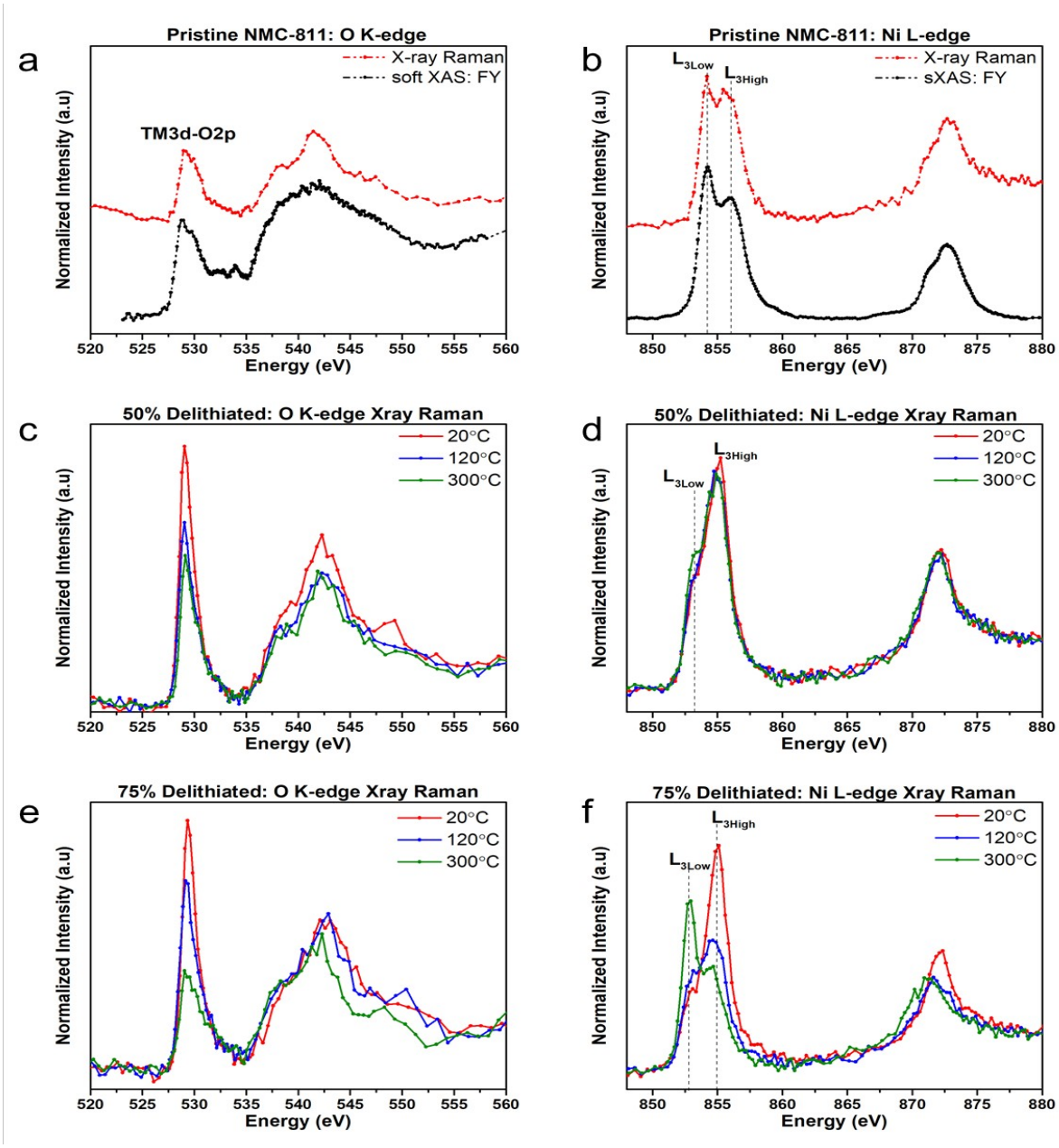

Figure 5. A comparison of the soft XAS data in FY mode to the Ni-L edge and O-K edge XRS spectra of pristine NMC-811 is shown in a) and b), respectively. In situ XRS data as a function of temperature (c, d) for the 50% delithiated NMC-811 sample and (e,f) for the 75% delithiated sample.

temperatures, as well as the reference spectra of standard TM oxides. The interpretation of this region of the O K-edge spectra in NMC materials is

complicated by the overlap of peaks, but the use of reference materials aids in interpretation. A peak indexing analysis was performed as was done in reference [21]. In the spectra, there are three peaks associated with (1) Ni^{3+} 3d-O2p hybridization similar to $LiNiO_2$ (grey), (2) Co^{3+} 3d-O2p hybridization as in $LiCoO_2$ (orange), and (3) an overlap of the Mn^{4+} 3d-O2p (teal) and Ni^{2+} 3d-O2p (pink) hybridization as in MnO_2 and NiO, respectively. Given the high Ni content in NMC-811, it is likely that the Ni-O covalency will contribute more to the intensity of the low energy region than that of Co or Mn.[31] After heating to 120 °C, both the 50% delithiated and 75% delithiated samples show an incremental rise in the intensity of the Ni^{3+} 3d-O2p peak, consistent with the trends seen in $L_{3high/low}$ intensity ratios for the Ni L-edge XAS data. However, for both samples heated to 200 °C (navy), this peak decreases significantly, while the Ni^{2+} 3d-O2p peak increases, consistent with both the Ni K-edge and L-edge XAS analysis. Although this peak also overlaps with the Mn^{4+} 3d-O2p feature, it is more reasonable to associate its intensification in the heated samples with a reduced Ni oxidation state than with increased Mn^{4+}content. This is further confirmed by its growth in samples heated above 300℃, where Ni reduction was demonstrated to occur using several different techniques.

To further examine bulk changes in the thermally exposed delithiated NMC-811 samples, presented for the first time, we employed operando X-ray Raman spectroscopy (XRS). This is a hard x-ray technique that combines the advantages of hard x-rays to probe hundreds of μm into the bulk of a sample with the improved sensitivity of soft XAS.[32,33] It is a photon-in/photon-out (PIPO) technique, which provides bulk sensitive information on low Z systems such as oxygen.[33,34] This is one major advantage of XRS over hard XAS. XRS spectra provide data pertaining to the local structure and element specific chemical bonds, while avoiding the saturation effects that occur in soft XAS FY mode.[32,35] XRS is an analogue of electron energy loss spectroscopy (EELS) but hard x-rays are used instead of electrons. Figures 5a and b show a comparison of soft XAS spectra in FY mode and XRS spectra for the pristine (as synthesized) NMC-811 for the Ni L-edge and O K-edge, respectively. The similarities between the two types of spectra are readily apparent. However, there are differences in the signal to noise ratio, because the X-ray Raman cross sections are up to five orders of magnitude weaker compared to direct XAS. Another difference is in the L_{3high}/L_{3low} ratios in the Ni L-edge data; for the soft XAS it is 0.79 and for the XRS spectra, it is 0.94. This can be attributed to the redox state gradient from surface to bulk induced by surface reconstruction and the differences in the penetration depths for the two types of experiments: 100 nm for soft XAS in FY mode and millimeters in for XRS.

Figure 5 c-f shows the Ni L-edge and O K-edge spectra at various temperatures. Based on the changes seen in the $L_{3high/low}$ intensity ratios

(Figures d, f), it is apparent that Ni is reduced at 300˚C for both samples, although the effect is greater for the 75% delithiated sample than the 50% delithiated sample, similar to what is seen in the XAS data. In contrast, little change is seen at 120˚C for the latter sample, whereas reduction of Ni is already apparent for the former. The apparent discrepancy with the XAS and other data can be explained by the differing conditions of these experiments; the XRS experiment was performed operando rather than ex situ, and required long collection times at elevated temperatures to ensure sufficient signal-to-noise ratios. This implies that phase conversion and concomitant metal reduction and oxygen evolution started to occur at significantly lower temperatures than what was observed in the faster experiments.

The low energy TM3d-O2p peaks in the O K-edge spectra (Figures 5 c and e) also reduce in intensity at 120°C for both delithiated samples. According to the XRD (Figure 1) and TGA data (Figure S4), phase transitions involving oxygen loss should not have yet occurred, but the Ni L-edge XRS data suggests otherwise. The intensity of this peak is also related to the concentration of hole states and is a measure of the covalency between the O 2p and antibonding metal orbitals.[36–38] Thus, another possible explanation, taken together with the Ni K-edge XANES data, which paradoxically shows apparent Ni oxidation at this temperature, is that electron density has moved away from the Ni ions and towards the O ions. Thus, these changes observed in the XRS and XAS data near 120˚C are subtle signs that phase changes are about to occur or have already initiated, even though they are not detectable in the XRD data. The more obvious decrease in intensity of the TM3d-O2p peaks at 300 °C, are, however, consistent with the conversion to spinel phases in the bulk, as observed in Figure 1.

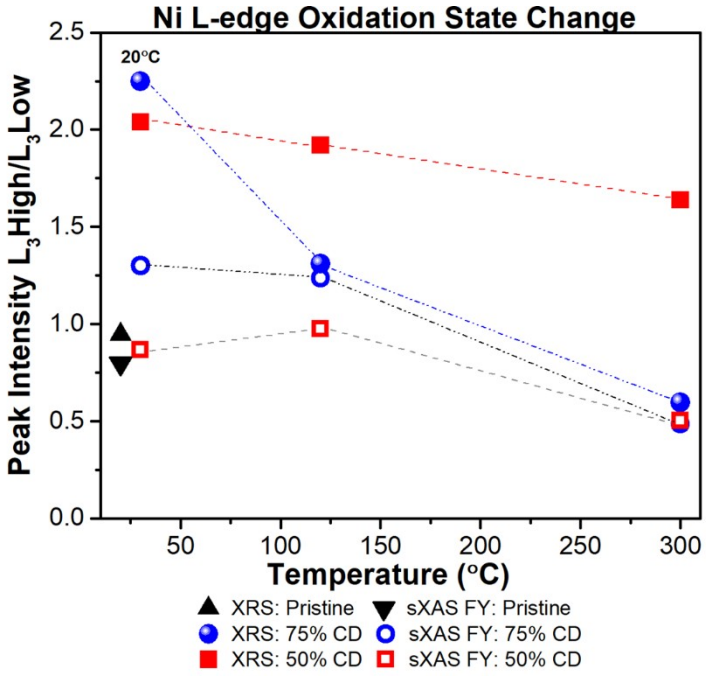

Figure 6. Comparison of the Ni $L_{3high/low}$ intensity ratios obtained from soft XAS (FY mode) and XRS experiments, as a function of

A summary of Ni L_{3high}/L_{3low} ratios (i.e., relative Ni oxidation states) obtained from the soft XAS and XRS experiments as a function of temperature is presented in Figure 6. Differences between XRS and soft XAS values for the three types of samples (pristine, 50% delithiated, and 75% delithiated) at room temperature are attributable to surface

reconstruction to a rocksalt phase, where metals at or near the surface are in a more reduced state than further into the bulk. Ni was continuously reduced in the bulk (XRS data) as the temperature was raised, with the effect more pronounced for the less thermally stable 75% delithiated sample than for the 50% delithiated material. The ex situ XAS data show more complex behavior, with a slight apparent oxidation for Ni at 120˚C, which may be due in part to redistribution of Li ions away from particle surfaces. The XAS experiment may also capture a different equilibrium state than the XRS data, which was performed operando. At 300˚C, the surfaces of both types of particles are significantly reduced. The oxidation states of Ni near the surface and in the bulk are nearly the same in the 75% delithiated material heated to this temperature, but a profound discrepancy exists for the 50% delithiated material with the surface Ni at a much lower oxidation state than in the bulk. This phenomenon is also observed for the data at 120˚C, and strongly implies that the surface is more reactive and less thermally stable than the bulk. Heating the 50% delithiated material induces considerable heterogeneity well before major phase transitions are observed using bulk techniques.

1.3.4. Chemical heterogeneity within secondary particles of NMC-811

To further understand the thermally-driven chemical behavior that occurs within the delithiated NMC-811 secondary particles, we applied temperature-controlled *operando* full-field transmission x-ray microscopy (TXM). Here we focused on the secondary particles and exposed them to various temperatures while concurrently collecting spectro-microscopic data over the Ni K-edge to extract 2D Ni valence maps (see Figure 7). The equipment has a nominal special resolution at 30 nm, which can probe the particle’s lateral heterogeneity at the sub-particle level.[22,39] Prior to chemical delithiation, the pristine NMC-811material was analyzed in Figure S8). The 2D Ni XANES valence maps and the extracted absorption spectra over selected regions of interest (as highlighted in the 2D XANES image) demonstrate the uniformity of the Ni oxidation state throughout the entire particles.

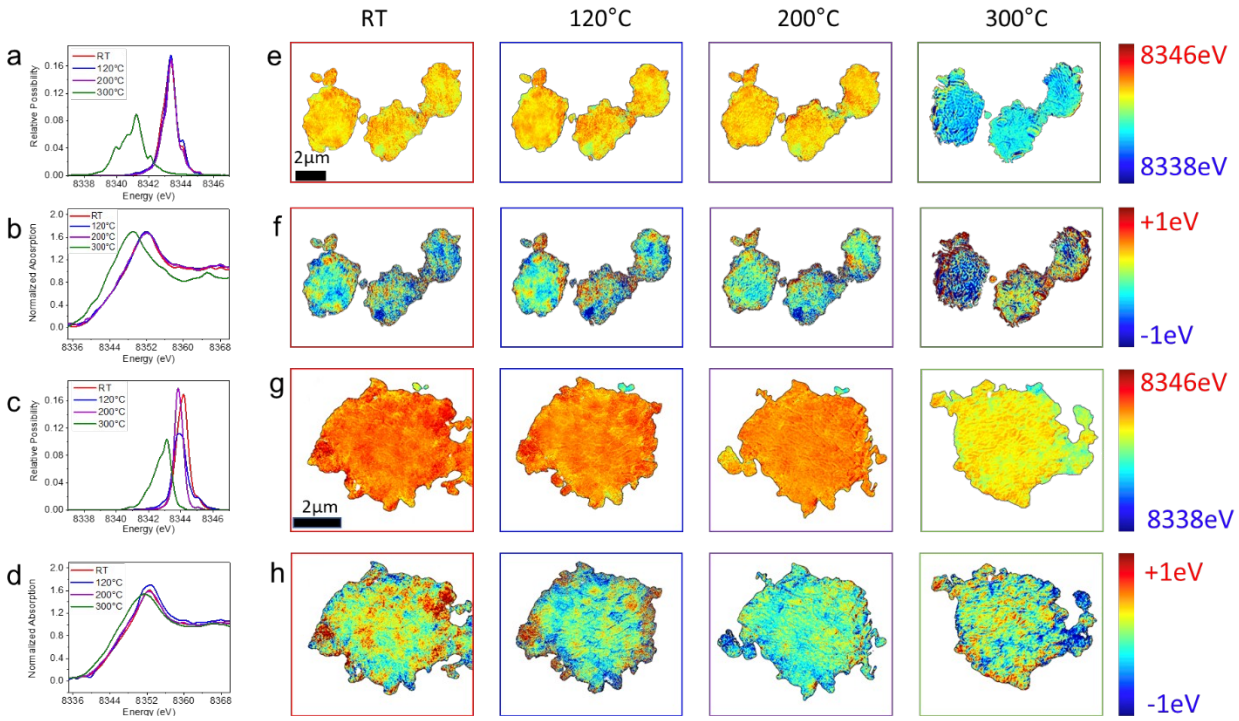

Figure 7. Full-field X-ray spectro-microscopy of delithiated NMC-811 samples during in-situ heating to 300°C as a function of temperature. Distributions of the Ni edge shift as a function of temperature and representative multiple pixel averaged XANES spectra for the 50% delithiated NMC-811 (a and b) and the 75% delithiated sample (c and d). 2D Ni K-edge mapping of a 50% delithiated NMC-811 particle as a function of temperature (e) and relative edge energy differences (f). 2D Ni K-edge mapping of a 75% delithiated NMC-811 particle as a function of temperature (g) and relative edge energy differences (h).

The average probability distribution of the Ni edge energy as a function of thermal exposure for the 50% delithiated and 75% delithiated samples are shown in Figure 7 a and e, respectively. There was little change in the Ni edge energy positions from room temperature to 200˚C. However, a significant shift toward lower energy occurred at 300˚C, especially for the 50% delithiated sample. This is in good agreement with the averaged Ni K-edge XANES spectra over the entire field of view (Figure 7b and f). Based on the color-coded legend, at room temperature, the 2D chemical map shows more oxidized Ni in the 75% delithiated sample compared to the 50% delithiated sample, as seen with the bulk XANES measurements in Figure 2. Even at room temperature, there was visible chemical heterogeneity within the secondary particles, attributable to the non-uniform removal of Li via chemical delithiation.[22,39] The 2D chemical maps are color-coded to the absolute value of the Ni XANES edge value in Figure 7 e and g, and as relative values in Figures 7 f and h, showing local Ni oxidation state changes

as a function of temperature. Based on Figure S8, the heterogeneity found within the particles is largely due to the chemical delithiation treatment (as demonstrated in our previous work [22]) as well as thermal exposure and not the result of inconstancies in the starting material. Local differences in Ni oxidation states are readily apparent in the heated samples. In particular, there are areas near particle surfaces that appear oxidized in the samples at 120℃, similar to what was detected in the soft XAS experiments in Figures 3 and 4. This further reinforces the theory that there is thermally driven rearrangement of Li ions in the secondary particles. This has also been proposed by Wei *et al.*, who have suggested that Li migration, oxygen release, and Ni redox occur in tandem during heating. [39] Furthermore, phenomenon has also been reported in several different cathode materials such as NMCs, Li-rich NMC, and NCA. [36,40,41]

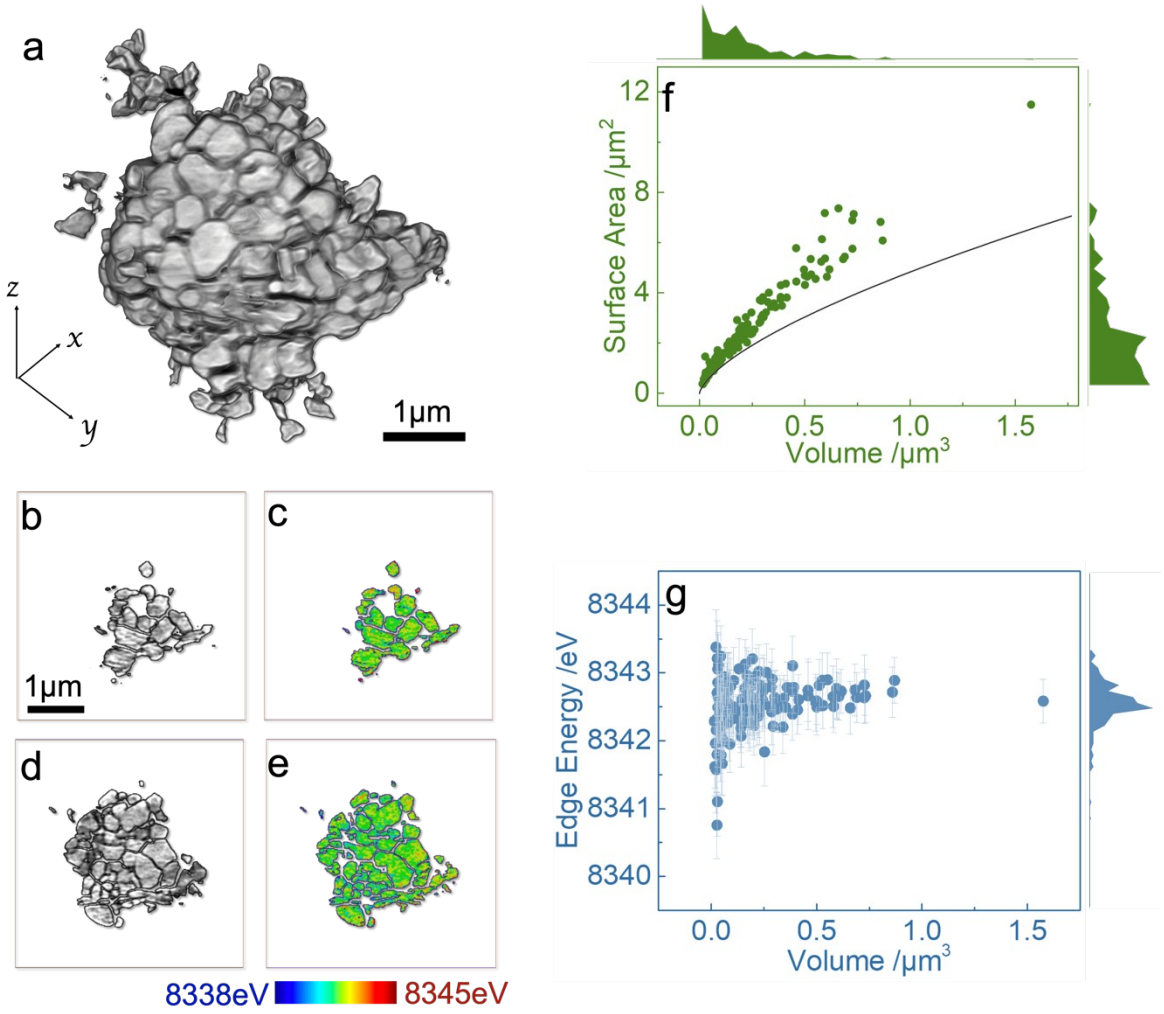

Figure 8. Three-dimensional (3D) XANES imaging and analysis of the 75% delithiated NMC-811 particle after heating to 300°C. (a) 3D rendering of the single energy tomographic analysis. (b,d) indicate virtual slices through different depths of the particle in the x-z plane while (c,e) are the corresponding XANES maps over the same virtual slices. The correlation analysis of the surface area and the Ni K-edge energy versus the primary particle volume are presented in f and g, respectively. The black line in f

TXM also allows the investigation of morphology changes as a function of temperature. The 75% delithiated sample underwent significant morphological changes at every temperature. Portions of the secondary particle detached during each temperature increment, probably due to thermally driven phase transformations resulting in oxygen release. Even at 120˚C, oxygen release occurred locally well before it was detected in other experiments such as TGA. In addition, the 300˚C 2D XANES edge energy maps indicate that the 50% delithiated particle was actually more reduced than the 75% delithiated one. This is clearly a function of particle size, given the abundant evidence that, in the bulk, the 50% delithiated sample is more thermally stable than the 75% sample. To further illustrate this, TXM 2D Ni

XANES maps were taken for several small particles found in the 75% delithiated sample after heating to 300˚C (Figure S9). Here the particles appear to be reduced to a similar degree as the 50% delithiated sample at 300˚C shown in Figure 7e.

Operando 2D Co XANES mapping on the 75% delithiated sample was also performed on a 75% delithiated particle (Figure S10). Given the much lower Co content compared to Ni for this sample, the signal to noise ratio of this experiment is not as high as for the Ni TXM experiments. Nevertheless, it is obvious that Co was also reduced at this temperature, with similar heterogeneities observed.

Three-dimensional (3D) XANES imaging was used to investigate a selected 75% delithiated NMC-811 particle after heating to 300˚C (Figure 8). Nano-resolution tomography was conducted at a number of x-ray energy levels over the Ni K-edge. The experimental details and the concept of 3D XANES mapping method can be found elsewhere.[42,43] The single energy tomographic result presented in Figure 8a clearly suggests that the nominal spatial resolution at ~30 nm is sufficient to resolve the primary particles that make up the imaged secondary particle. The virtual slices through different depths of the particle (Figure 8b, d) and the distribution of Ni K-edge energies over the corresponding slices (Figure 8 c, e) highlight the complexity of the primary particles in terms of size and local Ni valence states. A quantitative correlation analysis (Figure 8 f and g), based on the individual grains segmented from the 3D data shown in Figure 8a, was carried out to complement the direct visualization discussed above. The surface area to volume ratio is a commonly used parameter for describing the morphological complexity. To make it more useful, we overlaid our data points with a baseline calculated from spheres of different diameter (Figure 8f). It suggests that the small grains are more close to spheres, while the larger grains exhibits larger surface-to-volume ratio, suggesting a more complicated shape. The particle shapes may have an effect on the thermal behavior of the NMC-811. The degree of variation in the Ni K-edge energies decreased as the particle size increased (Figure 8g). Though the number of large particles are limited in Figure 8g, when comparing all of the TXM data for the 75% delithiated sample, there is a significant difference in Ni oxidation states between large particle found in Figure 7g and 8h to the small particles seen in Figure S9 and Figure 8h after thermal abuse. It is important to note that TXM is a localized characterization technique; therefore, several particles must be analyzed. Coupling the 3D XANES with the 2D XANES chemical mapping after thermal abuse allowed us to demonstrate the disparity in thermal stability among particle size.

1.3.5 Thermal behavior comparison of NMC-622 and NMC-811 at different SOC

Herein, we aim to highlight the differences in the dynamic thermal properties of NMC-622 [44] and NMC-811. The nickel content of these two

materials differ; however, their thermal behavior is distinct even though the Li content in the structures is the same (50% and 75% delithiated). Upon chemical delithiation, the 50% and 75% chemically delithiated NMC-811 samples contain a phase mixture of H2 and H3 (see supporting information) while the delithiated NMC-622 samples are single phase at these compositions, and appear to be more thermally stable in the bulk due to their lower Ni contents. Transformations to spinel and rock salt structures occur at higher temperatures than for the corresponding partially delithiated NMC-811 analogs. There is very little change in the bulk Ni and Co oxidation states for 50% delithiated NMC-622 up to 350˚C,[44] whereas the metals in 50% delithiated NMC-811 are more thermally sensitive and show changes well below this temperature. Reduction of Ni and Co in the bulk of the 75% delithiated NMC-622 occurs by 350˚C, consistent with phase transformations to reduced metal oxides. At the surface, oxidation of Ni is observed in the heated 50% delithiated NMC-622 sample up to 350˚C, which is partially charge-compensated by the reduction of Co. In contrast, the Ni in the delithiated NMC-811 samples oxidize slightly at the surface before significant reduction occurs at 200˚C. Little evidence is seen for the paradoxical surface oxidation of Ni at the surfaces of 75% delithiated NMC-622; instead slight reduction occurs by 170˚ C and more significant reduction by 350˚C. In summary, differences in the thermal characteristics of NMC-622 and NMC-811 are primarily in the onset temperatures of the phase changes the behavior at particle surfaces.

1.4 Conclusions

A suite of bulk and surface-sensitive techniques was used to study the thermal stability of two NMC-811 samples delithiated to different degrees. While in situ heating XRD experiments indicate that bulk phase changes occur at temperatures above 150˚C for 75% delithiated samples or 250˚C for 50% delithiated samples, other experiments indicate that subtle changes involving oxygen evolution and metal redox changes can occur at temperatures well below the points where bulk phase changes can be detected. Apparent oxidation of Ni near 120˚C, detected in surface sensitive soft XAS experiments, imply a thermally driven rearrangement of lithium ions. In addition, there are changes in covalency and/or bond lengths detected in hard XAS experiments at similar temperatures, which serve as subtle portents for bulk phase changes occurring at higher temperatures. A comparison of surface-sensitive XAS and bulk sensitive XRS data suggest that thermal decomposition is initiated at particle surfaces and propagates into the bulk. The temperatures at which thermal decomposition reactions also vary with the length of thermal exposure, as evidenced by differences in detection of oxygen evolution or metal reduction in experiments performed on different time scales. Another significant observation is the extreme sensitivity to particle size, with smaller particles exhibiting much worse thermal stability compared to larger ones. In short, the thermal behavior of Ni-rich NMC materials is extremely complex, involving structure

reorganization, Li migration, transition metal oxidation/reduction, oxygen release, and morphology changes with profound implications for the safety of cells containing them, particularly under conditions of abuse where thermal runaway can occur.

1.5 Acknowledgments

This work and analysis conducted at the Molecular Foundry were supported by the Assistant Secretary for Energy Efficiency and Renewable Energy, Office of Vehicle Technologies of the U.S. Department of Energy under Contract No. DE-AC02-05CH11231. This document was prepared as an account of work sponsored by the United States Government While this document is believed to contain correct information, neither the United States Government nor any agency thereof, nor the Regents of the University of California, nor any of their employees, makes any warranty, express or implied, or assumes any legal responsibility for the accuracy, completeness, or usefulness of any information, apparatus, product, or process disclosed, or represents that its use would not infringe privately owned rights. Reference herein to any specific commercial product, process, or service by its trade name, trademark, manufacturer, or otherwise, does not necessarily constitute or imply its endorsement, recommendation, or favoring by the United States Government or any agency thereof, or the Regents of the University of California. The views and opinions of authors expressed herein do not necessarily state or reflect those of the United States Government or any agency thereof or the Regents of the University of California. We would like to acknowledge the use of the Stanford Synchrotron Radiation Lightsource, SLAC National Accelerator Laboratory, that is supported by the U.S. Department of Energy, Office of Science, Office of Basic Energy Sciences under Contract No. DE-AC02-76SF00515. J.A. would like to thank Emil Kim for the authorized use of the table of contents figure.

Declarations of Interest: none

References

[1] N. Nitta, F. Wu, J.T. Lee, G. Yushin, Mater. Today 18 (2015) 252–264.

[2] J. Xu, F. Lin, M.M. Doeff, W. Tong, J. Mater. Chem. A 5 (2017) 874–901.

[3] A. Mayyas, D. Steward, M. Mann, Sustain. Mater. Technol. 19 (2019) e00087.

[4] N. Yabuuchi, T. Ohzuku, J. Power Sources 119–121 (2003) 171–174.

[5] C. Daniel, D. Mohanty, J. Li, D.L. Wood, in: AIP Conf. Proc., American Institute of Physics, 2014, pp. 26–43.

[6] Y. Ruan, X. Song, Y. Fu, C. Song, V. Battaglia, J. Power Sources 400

(2018) 539–548.

[7] J.R. Dahn, E.W. Fuller, M. Obrovac, U. von Sacken, Solid State Ionics 69 (1994) 265–270.

[8] L. Wu, K.-W. Nam, X. Wang, Y. Zhou, J.-C. Zheng, X.-Q. Yang, Y. Zhu, Chem. Mater 23 (2011) 8.

[9] S. Tobishima, J. Yamaki, J. Power Sources 81–82 (1999) 882–886.

[10] T. Dagger, V. Meier, S. Hildebrand, D. Brüggemann, M. Winter, F.M. Schappacher, (2018).

[11] C. Korepp, W. Kern, E.A. Lanzer, P.R. Raimann, J.O. Besenhard, M. Yang, K.-C. Möller, D.-T. Shieh, M. Winter, J. Power Sources 174 (2007) 637–642.

[12] J. Li, E. Murphy, J. Winnick, P.A. Kohl, The Effects of Pulse Charging on Cycling Characteristics of Commercial Lithium-Ion Batteries, n.d.

[13] J. Xu, F. Lin, M.M. Doeff, W. Tong, J. Mater. Chem. A 5 (2017) 874–901.

[14] K.-W. Nam, S.-M. Bak, E. Hu, X. Yu, Y. Zhou, X. Wang, L. Wu, Y. Zhu, K.-Y. Chung, X.-Q. Yang, Adv. Funct. Mater. 23 (2013) 1047–1063.

[15] S.M. Bak, E. Hu, Y. Zhou, X. Yu, S.D. Senanayake, S.J. Cho, K.B. Kim, K.Y. Chung, X.Q. Yang, K.W. Nam, ACS Appl. Mater. Interfaces 6 (2014) 22594–22601.

[16] S. Hwang, S.M. Kim, S.-M. Bak, S.Y. Kim, B.-W. Cho, K.Y. Chung, J.Y. Lee, E.A. Stach, W. Chang, Chem. Mater. 27 (2015) 3927–3935.

[17] W.E. Gent, Y. Li, S. Ahn, J. Lim, Y. Liu, A.M. Wise, C.B. Gopal, D.N. Mueller, R. Davis, J.N. Weker, J.-H. Park, S.-K. Doo, W.C. Chueh, Adv. Mater. 28 (2016) 6631–6638.

[18] X.. Yang, X. Sun, J. McBreen, Electrochem. Commun. 1 (1999) 227–232.

[19] W. Li, J.N. Reimers, J.R. Dahn, Solid State Ionics 67 (1993) 123–130.

[20] W.-S. Yoon, K.Y. Chung, J. McBreen, X.-Q. Yang, Electrochem. Commun. 8 (2006) 1257–1262.

[21] C. Tian, D. Nordlund, H.L. Xin, Y. Xu, Y. Liu, D. Sokaras, F. Lin, M.M. Doeff, J. Electrochem. Soc. 165 (2018) A696–A704.

[22] C. Tian, Y. Xu, D. Nordlund, F. Lin, J. Liu, Z. Sun, Y. Liu, M. Doeff, Joule 2 (2018) 464–477.

[23] F.M.F. De Groot, M. Grioni, J.C. Fuggle, J. Ghijsen, G.A. Sawatzky, H. Petersen, Phys. Rev. B 40 (1989) 5715–5723.

[24] M. Pedio, J.C. Fuggle, J. Somers, E. Umbach, J. Haase, T. Lindner, U. Hofer, M. Grioni, F.M.F. De Groot, U. Nj, T. Veld, E.D. Nijmegen, N.B.

Hillert, L. Becker, A. Robinson, Covalency in Oxygen Chemisorption as Probed by X-Ray Absorption NL-6525 ED Nijmegen, The Netherlands, n.d.

[25] F. Lin, Y. Liu, X. Yu, L. Cheng, A. Singer, O.G. Shpyrko, H.L. Xin, N. Tamura, C. Tian, T.-C. Weng, X.-Q. Yang, Y. Shirley Meng, D. Nordlund, W. Yang, M.M. Doeff, (n.d.).

[26] F. Lin, D. Nordlund, Y. Li, M.K. Quan, L. Cheng, T.-C. Weng, Y. Liu, H.L. Xin, M.M. Doeff, Nat. Energy 1 (2016) 15004.

[27] J. Zhu, G. Chen, J. Mater. Chem. A 7 (2019) 5463–5474.

[28] F. Lin, D. Nordlund, I. Markus, T.-C. Weng, H.L. Xin, M. Doeff, Energy Environ. Sci. (2014) 3077–3085.

[29] C.X. Kronawitter, J.R. Bakke, D.A. Wheeler, W.-C. Wang, C. Chang, B.R. Antoun, J.Z. Zhang, J. Guo, S.F. Bent, S.S. Mao, L. Vayssieres, Nano Lett. 11 (2011) 3855–3861.

[30] F.M.F. De Groot, M. Gnom, J.C. Fuggle, J. Ghijsen, G.A. Sawatzky, H. Petersen Berliner, Oxygen 1s X-Ray-Absorption Edges of Transition-Metal Oxides, n.d.

[31] W. Yoon, M. Balasubramanian, K.Y. Chung, X. Yang, J. Mcbreen, C.P. Grey, D.A. Fischer, W. Yoon, M. Balasubramanian, K.Y. Chung, (2005) 17479–17487.

[32] U. Bergmann, P. Glatzel, S.P. Cramer, Bulk-Sensitive XAS Characterization of Light Elements: From X-Ray Raman Scattering to X-Ray Raman Spectroscopy, 2002.

[33] D. Sokaras, D. Nordlund, T.-C. Weng, R.A. Mori, P. Velikov, D. Wenger, A. Garachtchenko, M. George, V. Borzenets, B. Johnson, Q. Qian, T. Rabedeau, U. Bergmann, Rev. Sci. Instrum 83 (2012) 43112.

[34] A. Nilsson, D. Nordlund, I. Waluyo, N. Huang, H. Ogasawara, S. Kaya, U. Bergmann, L.Å. Näslund, H. Öström, P. Wernet, K.J. Andersson, T. Schiros, L.G.M. Pettersson, J. Electron Spectros. Relat. Phenomena 177 (2010) 99–129.

[35] S. Huotari, T. Pylkkänen, R. Verbeni, G. Monaco, K. Hämäläinen, Nat. Mater. 10 (2011) 29.

[36] L. Mu, R. Lin, R. Xu, L. Han, S. Xia, D. Sokaras, J.D. Steiner, T.-C. Weng, D. Nordlund, M.M. Doeff, Y. Liu, K. Zhao, H.L. Xin, F. Lin, Nano Letters 18 (2018) 3241-3249.

[37] C. Ma, J. Alvarado, J. Xu, R.J. Clément, M. Kodur, W. Tong, C.P. Grey, Y.S. Meng, J. Am. Chem. Soc. 139 (2017) 4835–4845.

[38] S. Hy, W.-N. Su, J.-M. Chen, B.-J. Hwang, J. Phys. Chem. C 116 (2012)

25242–25247.

[39] C. Wei, Y. Zhang, S.-J. Lee, L. Mu, J. Liu, C. Wang, Y. Yang, M. Doeff, P. Pianetta, D. Nordlund, X.-W. Du, Y. Tian, K. Zhao, J.-S. Lee, F. Lin, Y. Liu, J. Mater. Chem. A 6 (2018) 23055–23061.

[40] S. Li, S.-J. Lee, X. Wang, W. Yang, H. Huang, D.S. Swetz, W.B. Doriese, G.C. O'Neil, J.N. Ullom, C.J. Titus, K.D. Irwin, H.-K. Lee, D. Nordlund, P. Pianetta, C. Yu, J. Qiu, X. Yu, X.-Q. Yang, E. Hu, J.-S. Lee, Y. Liu, J. Am. Chem. Soc. 141 (2019) 12079–12086.

[41] M.M. Besli, A.K. Shukla, C. Wei, M. Metzger, J. Alvarado, J. Boell, D. Nordlund, G. Schneider, S. Hellstrom, C. Johnston, J. Christensen, M.M. Doeff, Y. Liu, S. Kuppan, J. Mater. Chem. A 7 (2019) 12593–12603.

[42] F. Meirer, J. Cabana, Y. Liu, A. Mehta, J.C. Andrews, P. Pianetta, IUCr, J. Synchrotron Radiat. 18 (2011) 773–781.

[43] Y. Liu, F. Meirer, P.A. Williams, J. Wang, J.C. Andrews, P. Pianetta, IUCr, J. Synchrotron Radiat. 19 (2012) 281–287.

[44] C. Tian, Y. Xu, W. H. Kan, D. Sokaras, D. Nordlund, H. Shen, K. Chen, Y. Liu, M. M. Doeff, submitted. (2019)

Supporting Information

Thermal stress-induced charge and structure heterogeneity in emerging cathode materials

Judith Alvarado,[1‡] Chenxi Wei,[2,3‡] Dennis Nordlund,[3] Thomas Kroll,[3] Dimosthenis Sokaras,[3] Yangchao Tian[2], Yijin Liu,[3*] Marca M. Doeff[1*]

1. Energy Storage & Distributed Resources Division, Lawrence Berkeley National Laboratory, Berkeley, California 94720, USA

2. National Synchrotron Radiation Laboratory, University of Science and Technology of China, Hefei, Anhui 230027, Chin

3. Stanford Synchrotron Radiation Lightsource, SLAC National Accelerator Laboratory, Menlo Park, California 94025, USA

* email: mmdoeff@lbl.gov, liuyijin@slac.stanford.edu

‡ These authors contributed equally

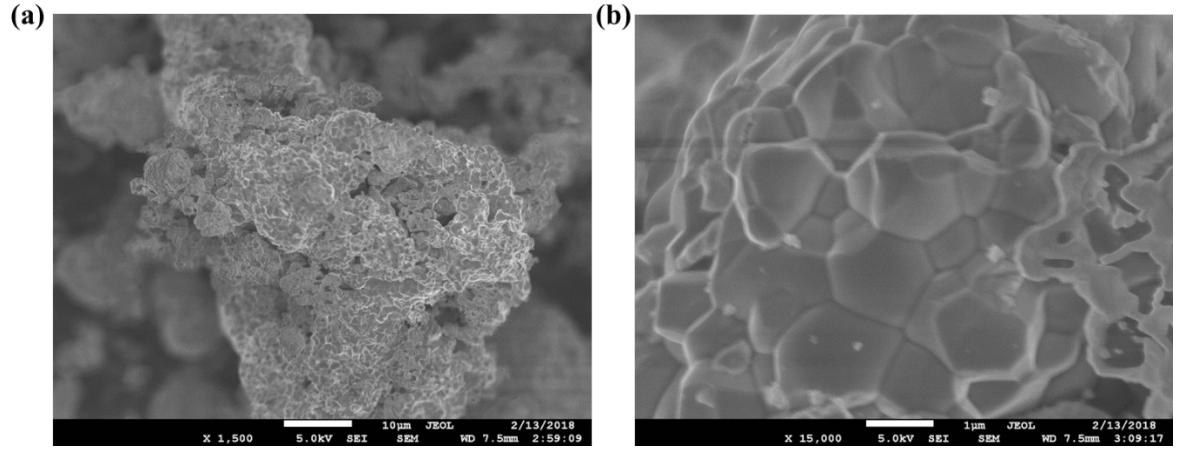

Figure S1. Scanning electron microscopy images of the pristine NMC-811.

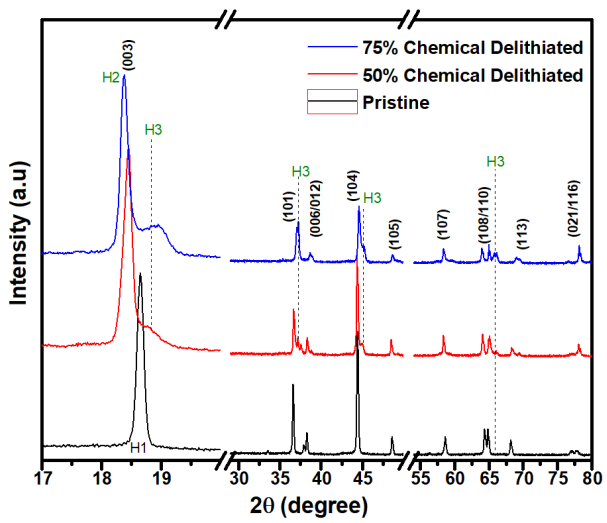

Figure S2. Ex-situ X-ray diffraction patterns of chemically delithiated NMC-811 samples.

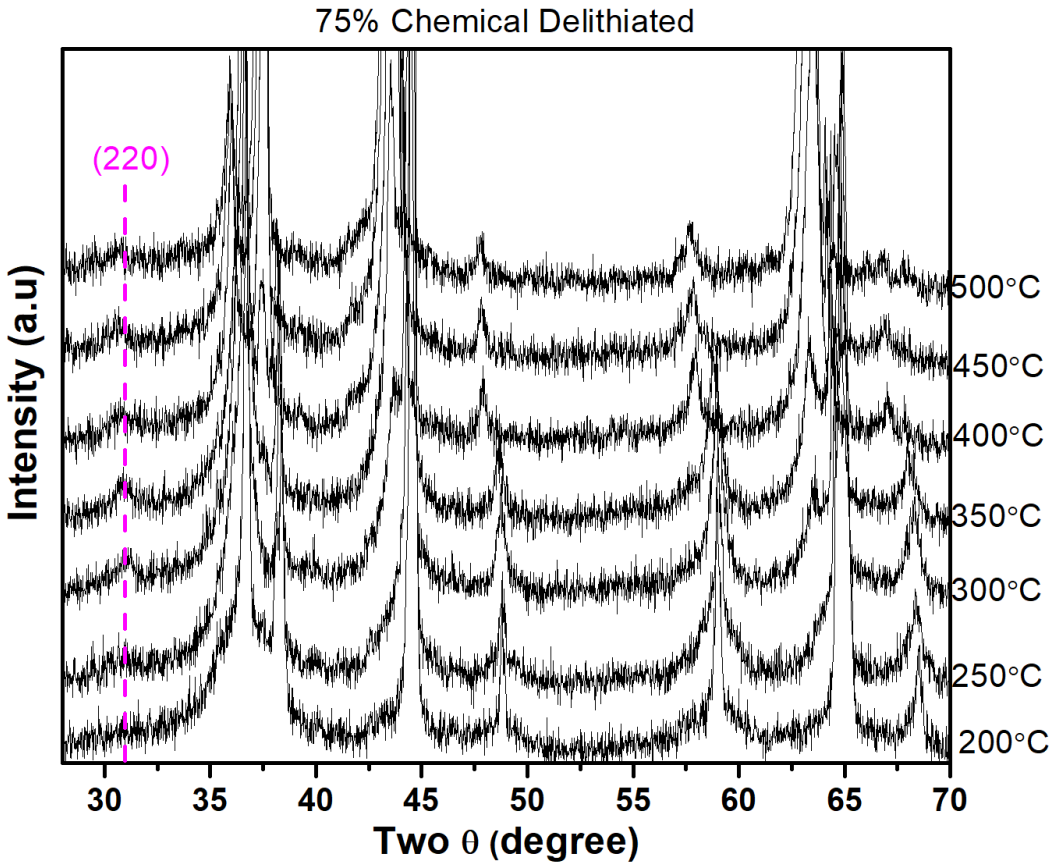

Figure S3. Zoomed in in-situ x-ray diffraction patterns of 75% delithiated NMC-811 from Figure 1b in the main text. The (220) reflection of the M_3O_4 spinel phase emerges near 250 °C.

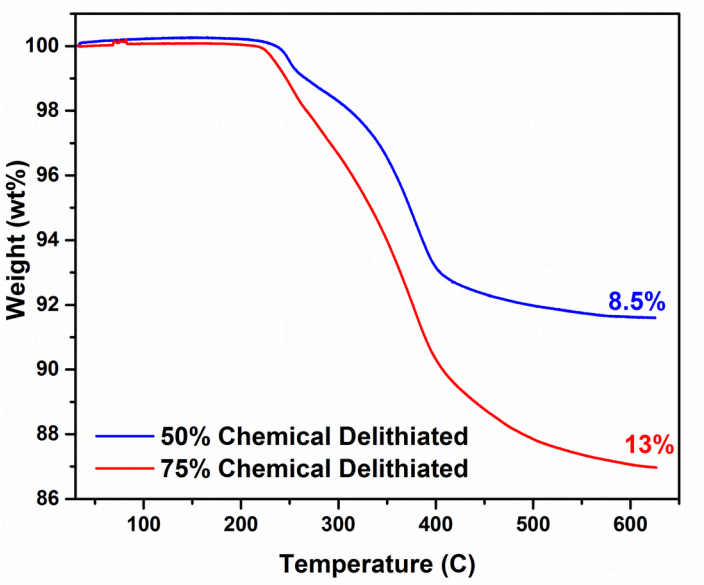

Figure S4. Thermogravimetric analysis of NMC-811 delithiated to 50% and 75%.

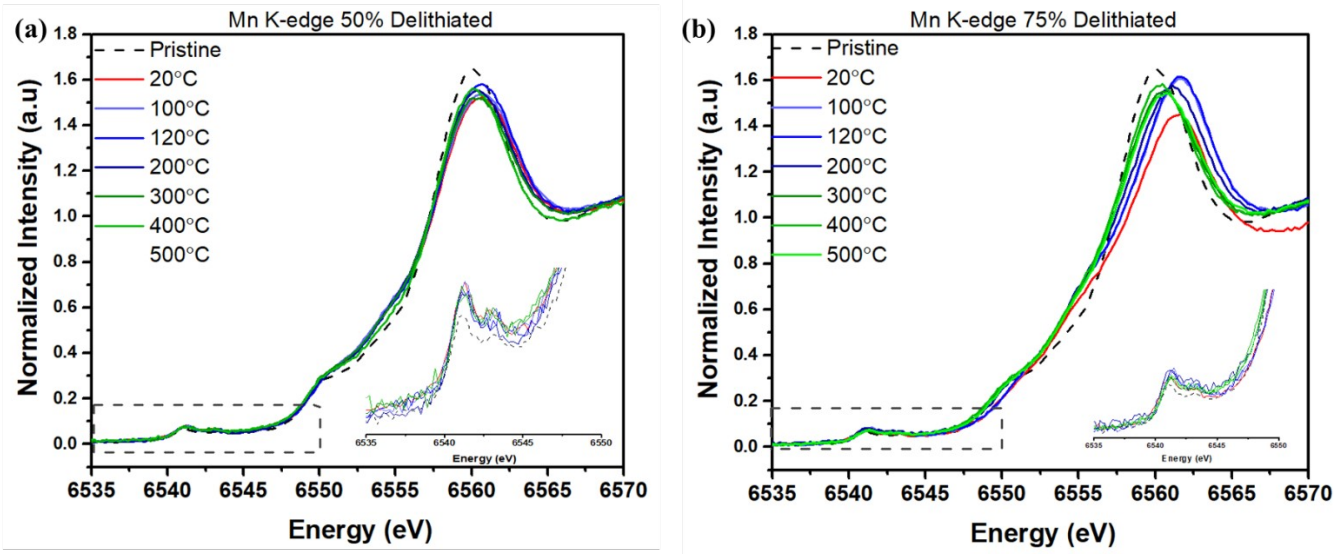

Figure S5. Post heating x-ray absorption spectroscopy XANES measurements of Mn K-edge of the (a) 50 % delithiated and (b) 75% delithiated samples.

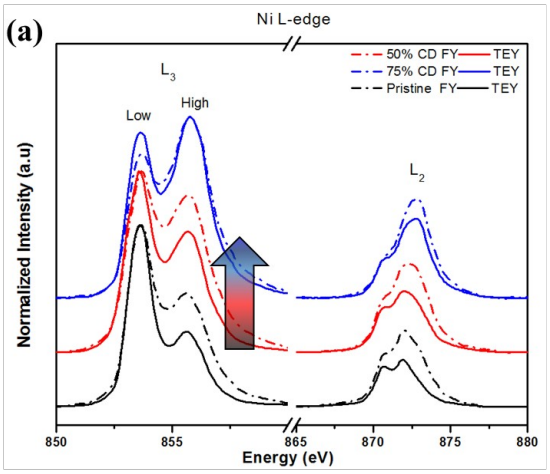
(a)
Ni L-edge
50% CD FY
TEY
75% CD FY
TEY
Pristine FY
TEY
L3
Low
High
L2
Normalized Intensity (a.u)
850
855
865
870
875
880
Energy (eV)

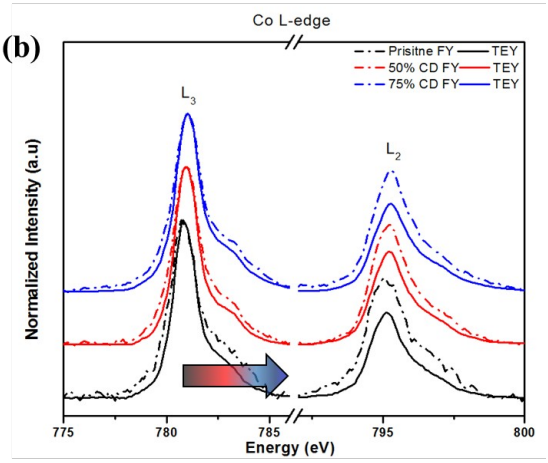
(b)
Co L-edge
Prisitne FY
TEY
50% CD FY
TEY
75% CD FY
TEY
L3
L2
Normalized Intensity (a.u)
775
780
785
795
800
Energy (eV)

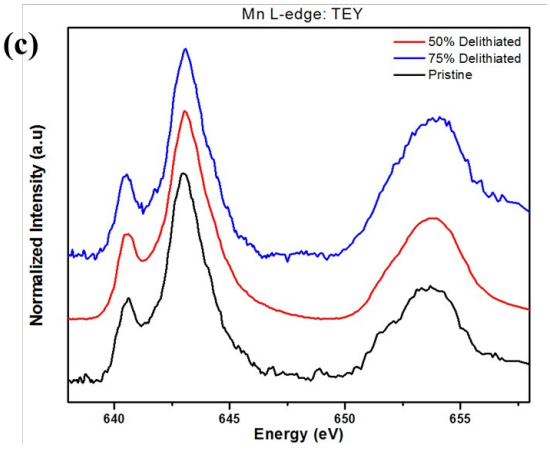
(c)
Mn L-edge: TEY
50% Delithiated
75% Delithiated
Pristine
Normalized Intensity (a.u)
640
645
650
655
Energy (eV)

Figure S6**.** Soft X-ray absorption spectroscopy measurements of (a) Ni L-edge, (b) Co L-edge and (c) Mn L-edge before thermal treatment. The TEY mode data is shown as a solid line and the FY mode data is presented as a dashed line.

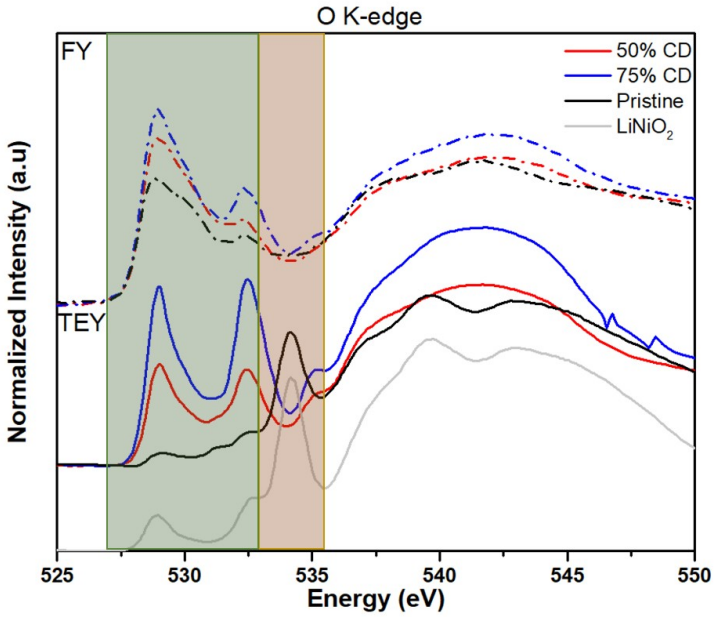

Figure S7**.** Soft X-ray absorption spectroscopy measurements of the O K-edge of pristine and delithiated samples before thermal treatment. TEY data is shown as solid lines and FY data is presented as dashed lines.

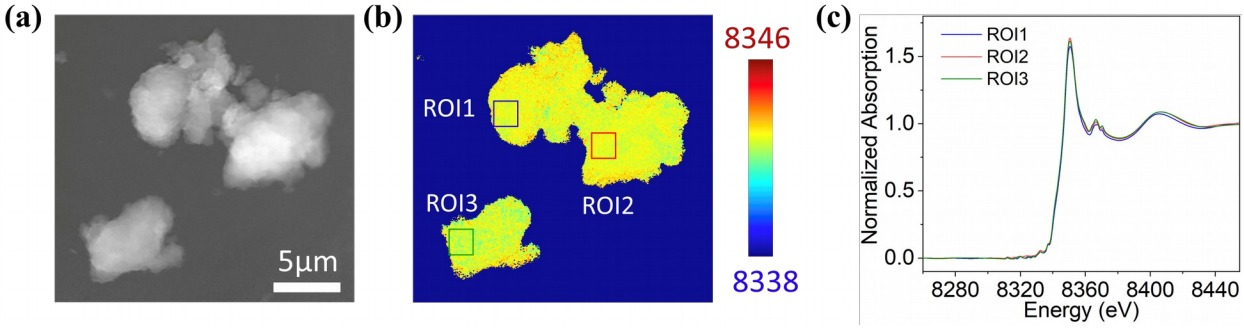

Figure S8. (a) The projection image and (b) is the corresponding 2D XANES image of the pristine NMC-811 cathode material. (c) Demonstrates the absorption spectra corresponding to the boxes from the 2D XANES image found in (b).

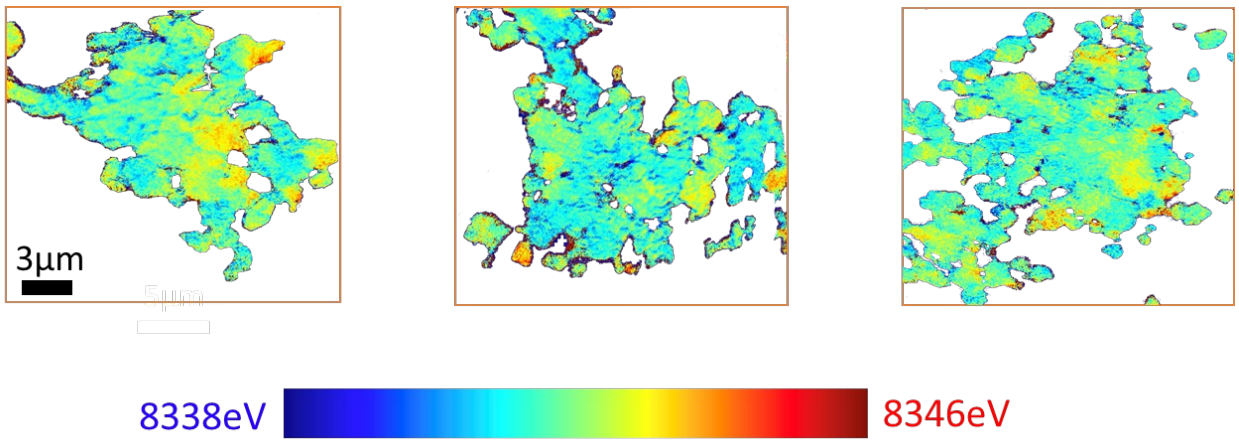

Figure S9. Post heating 2D TXM analysis on small 75% chemically delithiated NMC-811 particles, after heating to 300°C. The boxes indicate different field of views.

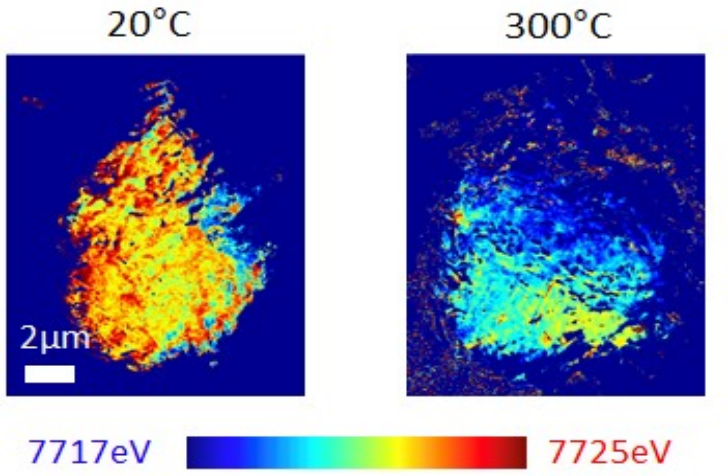

Figure S10. 2D XANES imaging of a 75% chemical delithiated NMC 811 particle before in-situ heat treatment after heating to 300°C.